ORIGINAL ARTICLE

Morphology and optoelectronic characteristics of organic field-effect transistors based on blends of polylactic acid and poly(3-hexylthiophene)

Chia-Jung Cho[1,2] · Shu-Yuan Chen[1] · Chi-Ching Kuo ●[1,2] · Loganathan Veeramuthu[1] · Ai-Nhan Au-Duong[1] · Yu-Cheng Chiu[3] · Shang-Hung Chang[4]

Abstract

This study investigates the influence of the solvent used to prepare films of a poly(3-hexylthiophene) (P3HT) and poly(lactic acid) (PLA) blend on the morphology and charge transport mobility of field-effect transistors (FETs). Films prepared from CH_2Cl_2, a poor solvent for P3HT, tended to form well-defined nanowires, attributable to P3HT self-assembly via a solubility-induced process. This phenomenon resulted in a mobility of 5.30×10^{-3} cm^2 (Vs)$^{-1}$ and an on/off ratio of 3.23×10^3 in a CH_2Cl_2-solvent P3HT/PLA-blend system with a P3HT content of 10 wt%. Even a blend with 2 wt% P3HT exhibited a mobility of 1.76×10^{-3} cm^2 (Vs)$^{-1}$. However, in blend systems where $CHCl_3$ solvent was employed in film preparation, the mobility decreased as the PLA content increased, and almost no electrical characteristics were exhibited at 50 wt% P3HT due to the isolated, spherical, phase-separated morphology of P3HT aggregation. Moreover, in CH_2Cl_2 solvent systems, the mobility of the P3HT/PLA (10/90) blend decreased from 5.3×10^{-3} cm^2 (Vs)$^{-1}$ (in a glove box) to 3.7×10^{-3} cm^2 (Vs)$^{-1}$ (after 28 days of air exposure), whereas that of 100 wt% P3HT declined by approximately one order of magnitude. These results confirm that P3HT/PLA blends prepared from CH_2Cl_2 solvent can be used to fabricate environmentally friendly, low-cost FETs with favorable air stability.

Introduction

Organic field-effect transistors (OFETs) based on conjugated polymers have received considerable research attention due to their solution processability, low cost, and flexibility [1–9]. Most polymer field-effect transistors (FETs) are used in microelectronic devices, such as smart cards, simple displays, sensors, and electronic barcodes

[10–14]. Among conjugated polymers, regioregular poly(3-hexylthiophene) (P3HT) has been widely investigated as an active material for use in OFETs due to its processability, preferential two-dimensional ordering of polymer chains, and outstanding charge transport characteristics [9, 15–18].

However, P3HT has been difficult to apply as a replacement for inorganic thin-film transistors because of its price and poor air stability. Because of the polymeric long-chain backbone and conjugated rigidity of P3HT, solution-processed semiconducting polymers require sufficient casting time to form highly π-conjugated structures along the source/drain (S/D) electrodes in polymer FETs. Additionally, a well-controlled interface between the organic semiconductor and gate insulator is essential for device

---

These authors contributed equally: Chia-Jung Cho, Shu-Yuan Chen.

✉ Chi-Ching Kuo
  kuocc@mail.ntut.edu.tw

✉ Shang-Hung Chang
  afen.chang@gmail.com

[1] Institute of Organic and Polymeric Materials, National Taipei University of Technology, Taipei 10608, Taiwan

[2] Research and Development Center for Smart Textile Technology, National Taipei University of Technology, Taipei 10608, Taiwan

[3] Department of Chemical Engineering, National Taiwan University of Science and Technology, Taipei 106, Taiwan

[4] Division of Cardiology, Department of Internal Medicine, Chang Gung Memorial Hospital-Linkou, Chang Gung University College of Medicine, Tao-Yuan, Taiwan

performance because charge transport occurs near the dielectric within a layer that is several nanometers thick [19, 20]. A simple innovation to maintain the electronic properties, lower costs, and improve other properties may be to blend two or more polymers that can protect P3HT from oxygen and moisture [21]. Such blends could combine the electrical characteristics of semiconducting polymers and the desired mechanical properties of nonconjugated materials. However, previously created blends have shown reduced electrical performance because the insulating components diluted the semiconducting characteristics of the conjugated polymers.

Goffri et al. reported using a vertical phase structure to first control the semiconducting polymer crystallization in molten, insulating semicrystalline polystyrene to prevent the electrical degradation of P3HT when blended with other polymers [22]. Studies have also reported findings on crystalline/crystalline blends such as P3HT/PEG [16], P3HT/HDPE [23], P3HT/PFO [22], P3HT/DH4T [24], P3HT/PVDF [25], and P3HT/P3DT [26]. Moreover, Bao's group has reported the FET performances of binary systems using high-mobility donor-acceptor type semiconducting polymers [27]. The crystalline/crystalline blend approach preserves the connectivity of the conjugated polymer and achieves high carrier mobility using only a small quantity of P3HT. Another previously reported method creates blends of crystalline and amorphous polymers, such as P3HT/a-PS and P3HT/PMMA [28–31]. When this method was used, the operating voltage could be lowered, thus increasing the capacitance of the gate dielectric. In addition, recent studies have reported several blends of conjugated polymers and insulators shown to have improved environmental stability and electrical properties [16, 23, 29, 32–35]. Researchers have reported the formation and embedding of networks of P3HT nanowires in an amorphous polymer matrix to address the low solubility of P3HT in a marginal solvent. When this method was applied, the solubility-induced nanowires adopted an edge-on orientation to the substrates, thus benefiting the charge transport of the OFETs [29, 35–37]

Polylactic acid (PLA) is a biodegradable biopolymer with good cell compatibility and is derived from corn and starch. PLA has biomedical applications and, most importantly, is nontoxic to human beings and the environment. Recently, PLA has been widely applied in drug delivery, tissue engineering, food packing, and bottles to reduce environmental impacts [38–40]. Thus, PLA is a green polymer material to use in FETs based on blended P3HT systems. However, few studies have examined the relationship between the electronic properties of PLA and conjugated polymer blends containing PLA. Although many research groups have studied P3HT-b-PLA [41, 42],

binary blends incorporating both P3HT and PLA for use in thin-film OFETs have been less investigated.

In this study, we report the effects of various solvents on the morphology and optoelectronic characteristics of OFETs based on P3HT/green polymer PLA blends. A series of binary blends of P3HT and PLA were prepared using processing solvents (a marginal solvent for P3HT, dichloromethane (CH_2Cl_2), and a good solvent for P3HT, chloroform ($CHCl_3$)) and compared. The phase-separated morphology of P3HT and the electrical characteristics and performance of the P3HT-PLA-blend-based OFETs were examined.

Experimental section

Materials

P3HT (Mw ≈ 50,000 g mol^{-1}, 90–95% regioregular) was used as received from Reike Metals Inc. (Lincoln, USA). PLA (polymer 2002D) (Mw ≈ 60,000 g mol^{-1}) was used as received from NatureWorks (Minnetonka, MN, USA). Anhydrous $CHCl_3$ (Aldrich), CH_2Cl_2 (Sigma-Aldrich), and phenyltrichlorosilane (PTS, Sigma-Aldrich) were used as received without further purification.

Device fabrication

The OFETs were fabricated on a highly doped n-type Si substrate with a thermally grown SiO_2 layer (300 nm, capacitance = 10 nF cm^{-2}). PTS was used as a silane coupling agent to modify the SiO_2 surface through the following process: A clean substrate was immersed in a 10 mM solution of PTS in anhydrous toluene at room temperature for 2 h. A series of binary blends of P3HT and PLA were prepared in CH_2Cl_2 or $CHCl_3$, and 1 wt% of these blended polymer solutions was annealed at 60 °C for 1 h. The solutions were then stored in a glove box for 12 h. Before coating, the solutions were filtered using 0.22 μm syringe filters. Thin films were spin-coated from the concentrated solutions at a spin rate of 1000 rpm for 60 s onto the PTS-treated SiO_2/Si substrate. Residual solvent was removed by heating the samples in nitrogen atmosphere for 1 h at 100 °C. The top-contact S/D regions were defined by a gold electrode (100 nm) through a regular shadow mask, and the channel length (L) and width (W) were 50 and 1000 μm, respectively. The output and transfer characteristics of the devices were measured using a Keithley 4200 semiconductor parametric analyzer, which was placed in the nitrogen-filled glove box. All OFETs showed typical p-type I–V characteristics during accumulation-mode operation. The field-effect mobility was estimated based on the saturated transfer characteristics of the device. $(I_d)^{0.5}$ versus V_g
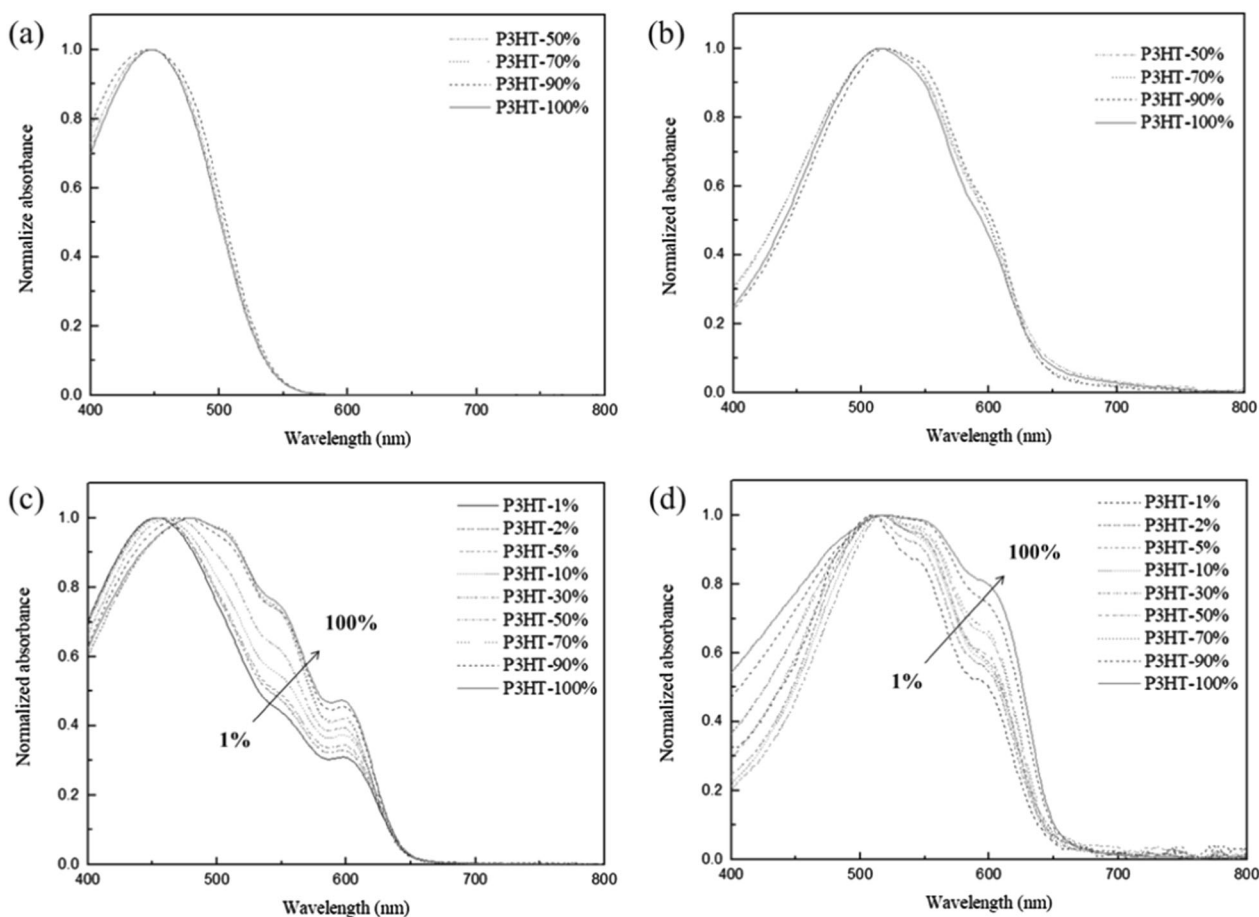
Fig. 1 UV-vis absorption spectra of P3HT/PLA blends in the solution state in **a** CHCl$_3$ and **b** CH$_2$Cl$_2$; UV-vis absorption spectra of P3HT/PLA-blend films prepared from **c** CHCl$_3$ and **d** CH$_2$Cl$_2$ solutions

Fig. 2 SEM images of P3HT/PLA blends prepared from CHCl$_3$ for P3HT contents of **a** 100%, **b** 90%, **c** 70%, and **d** 50%
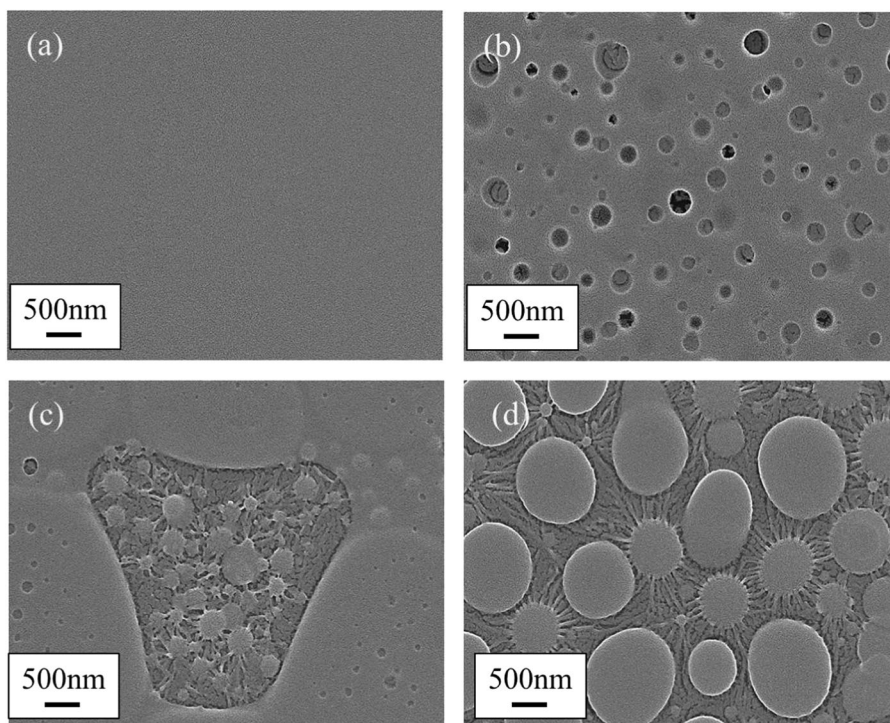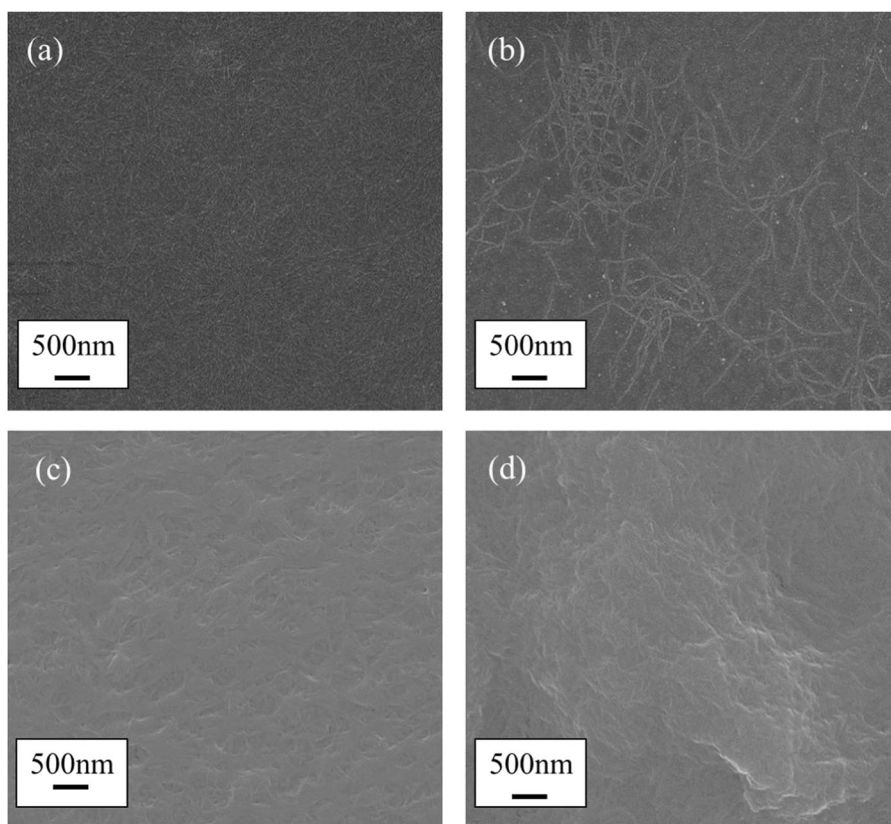
Fig. 3 SEM images of P3HT/
PLA blends prepared from
CH$_2$Cl$_2$ for P3HT contents of **a**
100%, **b** 90%, **c** 70%, and **d**
50%

was plotted using the following equation [16]:

$$I_d = \frac{WC_o\mu_h}{2L}(V_g - V_t)^2, \tag{1}$$

where I_d is the drain current, V_g is the gate voltage, V_t is the threshold voltage, μ_h is the hole mobility, and C_o is the capacitance of the gate insulator per unit area (SiO$_2$, 300 nm, $C_o = 10$ nF cm^{-2}). Figure S1 (supporting information) illustrates the device fabrication process.

Characterization

Thermogravimetric analysis (TGA) and differential scanning calorimetry (DSC) measurements were performed under nitrogen atmosphere at heating rates of 10 and 5 °C min^{-1} using TA instruments Q-50 and Perkin-Elmer DEC-7 analyzers, respectively. Ultraviolet–visible (UV-vis) absorption spectra were recorded using a Hitachi UV-3600 spectrophotometer (Shimadzu). To obtain the absorption spectrum of the thin film, 1 wt% polymer solution in CH$_2$Cl$_2$ or CHCl$_3$ was filtered through a 0.22-μm syringe filter and then spin-coated at a rate of 1000 rpm for 60 s onto a quartz substrate. The cast films were dried at 100 °C for 1 h in nitrogen atmosphere to remove residual solvent. Transmission electron microscopy (TEM) was performed using a JEOL 1230 microscope (Model JEM-1230)

operated at an acceleration voltage of 100 kV. The morphology of the polymer film surface was observed using a field-emission scanning electron microscope (FE-SEM, Model JSM-6330F, JEOL Ltd.) at an accelerating voltage of 10 kV. The samples were sputtered with Pt. The transfer and output characteristics of the OFETs were then determined using an electronic semiconductor parametric analyzer (Keithley 4200, Model 4200-SCS, Keithley Instruments Inc.).

P3HT/PLA-blend properties

The thermal properties of P3HT, PLA, and their blends were characterized. Figure S2 presents the DSC curves for blends of various ratios ((a) pristine-P3HT, (b) P3HT/PLA (90/10), (c) P3HT/PLA (50/50), and (d) pristine-PLA). The thermal properties of the blends are summarized in Table S1. The crystallization and melting temperatures of P3HT ($T_{c(P3HT)}$ and $T_{m(P3HT)}$) were 229.5 and 166.5 °C, respectively, and those of the P3HT/PLA blends were similar to those of pristine P3HT, indicating that blending with PLA did not suppress the crystalline characteristics of P3HT. The thermal decomposition temperatures (T_d, 95% residue) of P3HT and PLA were 453 and 328 °C, respectively, as shown in Fig. S3 and Table S1, indicating the favorable thermal stability of the blended system.

Fig. 4 SEM images of P3HT/PLA blends prepared from CH_2Cl_2 for P3HT contents of **a** 30%, **b** 10%, **c** 5%, **d** 2%, **e** 1%, and **f** 0%
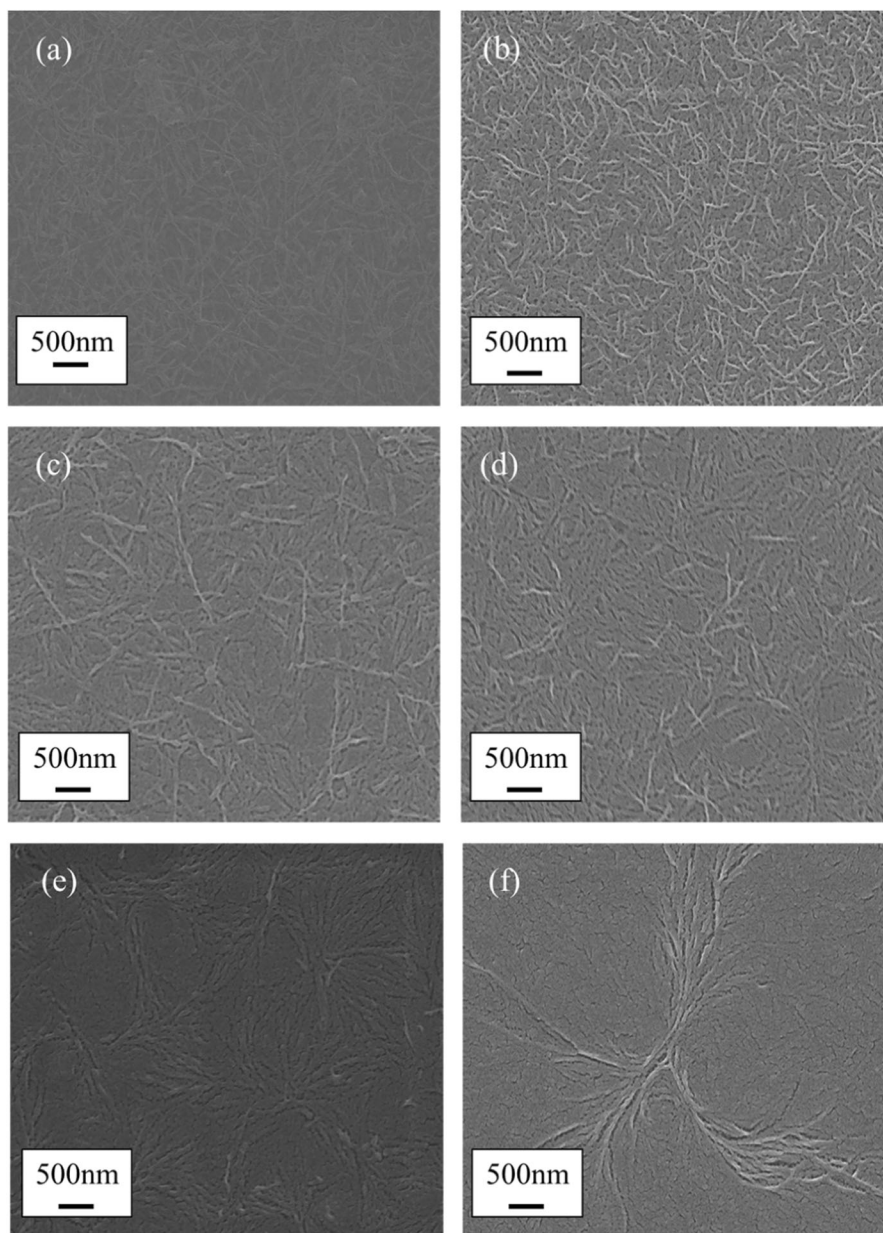
The UV-vis absorption spectra of P3HT/PLA-blend solutions of various ratios using $CHCl_3$ and CH_2Cl_2 as solvents are shown in Fig. 1a, b, respectively. The spectra of pristine P3HT and P3HT/PLA blends in $CHCl_3$ display a single absorption peak at a wavelength (λ_{max}) of 447 nm. This result can be attributed to the dissolved P3HT chains. Both P3HT and PLA dissolved well in $CHCl_3$. However, when CH_2Cl_2 was used, which is a marginal solvent for P3HT, three absorption bands with λ_{max} values of 480, 550, and 600 nm were obtained, which resulted from the strong interchain π–π stacking of P3HT [43], as shown in Fig. 1b. The absorption peak at 600 nm was attributed to the strong interchain π–π stacking of P3HT, which other studies have reported [44]. According to these results, the low solubility

of P3HT in CH_2Cl_2 may have induced polymer chain aggregation. Figure 1c, d presents the UV-vis absorption spectra of thin-film P3HT/PLA blends prepared from $CHCl_3$ and CH_2Cl_2, respectively. The UV-vis absorption spectra in solution show an absorption peak (Fig. 1a). By contrast, the UV-vis absorption spectra of $CHCl_3$-based pristine P3HT and P3HT/PLA blend thin films (Fig. 1c) have two shoulder absorption peaks at λ_{max} values of 520 and 600 nm. Furthermore, the results show that λ_{max} was redshifted from 447 nm to 520 nm from the solution state to the thin-film state. Therefore, slight π–π stacking of the P3HT chains occurred only in the P3HT/PLA thin films, not in $CHCl_3$ solutions. As shown in Fig. 1d, the UV-vis absorption spectra of CH_2Cl_2-based pristine P3HT and

Fig. 5 TEM images of P3HT/
PLA blends prepared from
CHCl$_3$ for P3HT contents of **a**
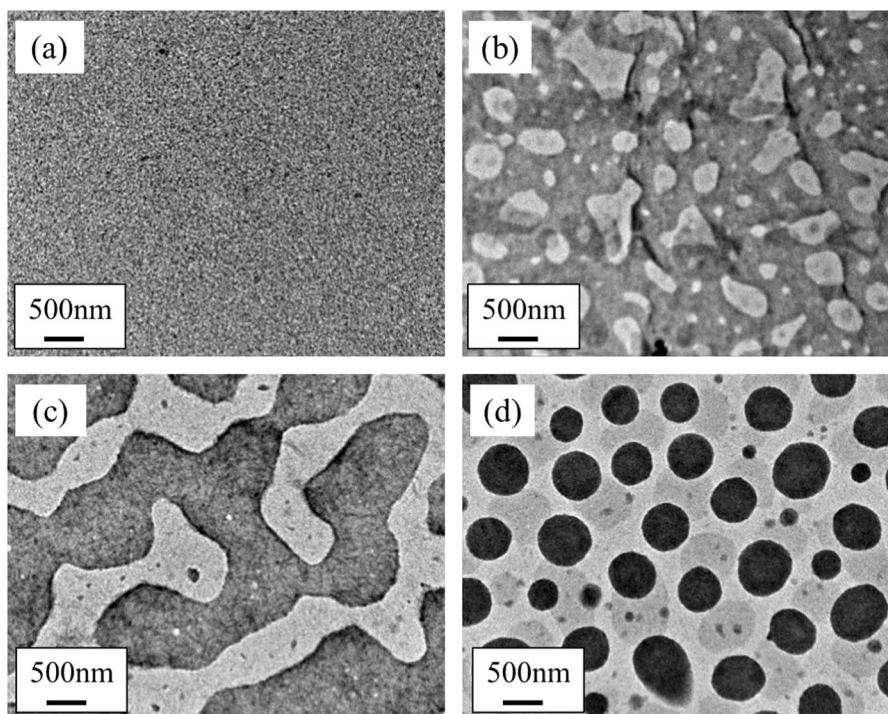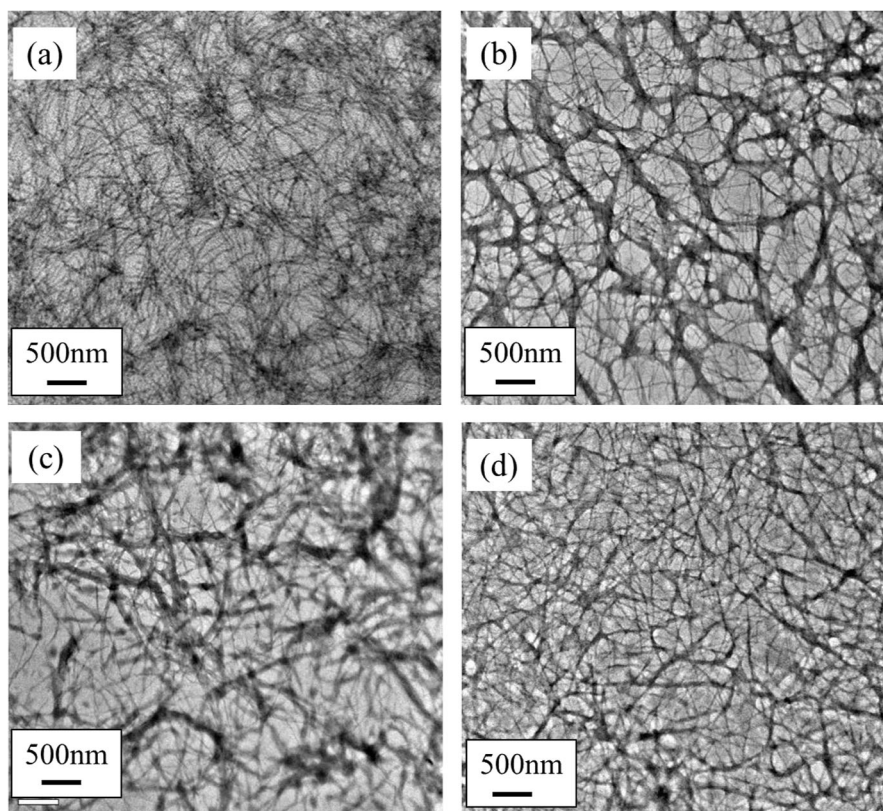100%, **b** 90%, **c** 70%, and **d**
50%

Fig. 6 TEM images of P3HT/
PLA blends prepared from
CH$_2$Cl$_2$ for P3HT contents of **a**
100%, **b** 90%, **c** 70%, and **d**
50%

P3HT/PLA-blend thin films exhibit three strong absorption bands at λ_{max} values of 480, 550, and 600 nm, resulting from the strong interchain π–π stacking of P3HT. The thin films of P3HT/PLA blends exhibited absorption spectra similar to those of the polymer blends in CH$_2$Cl$_2$, suggesting that the molecular packing of polymer chains may be similar in the thin film and solution. The intensities of the absorption peaks at 550 nm and 600 nm decreased when the

Fig. 7 TEM images of P3HT/PLA blends prepared from CH$_2$Cl$_2$ for P3HT contents of **a** 30%, **b** 10%, **c** 5%, **d** 2%, **e** 1%, and **f** 0%
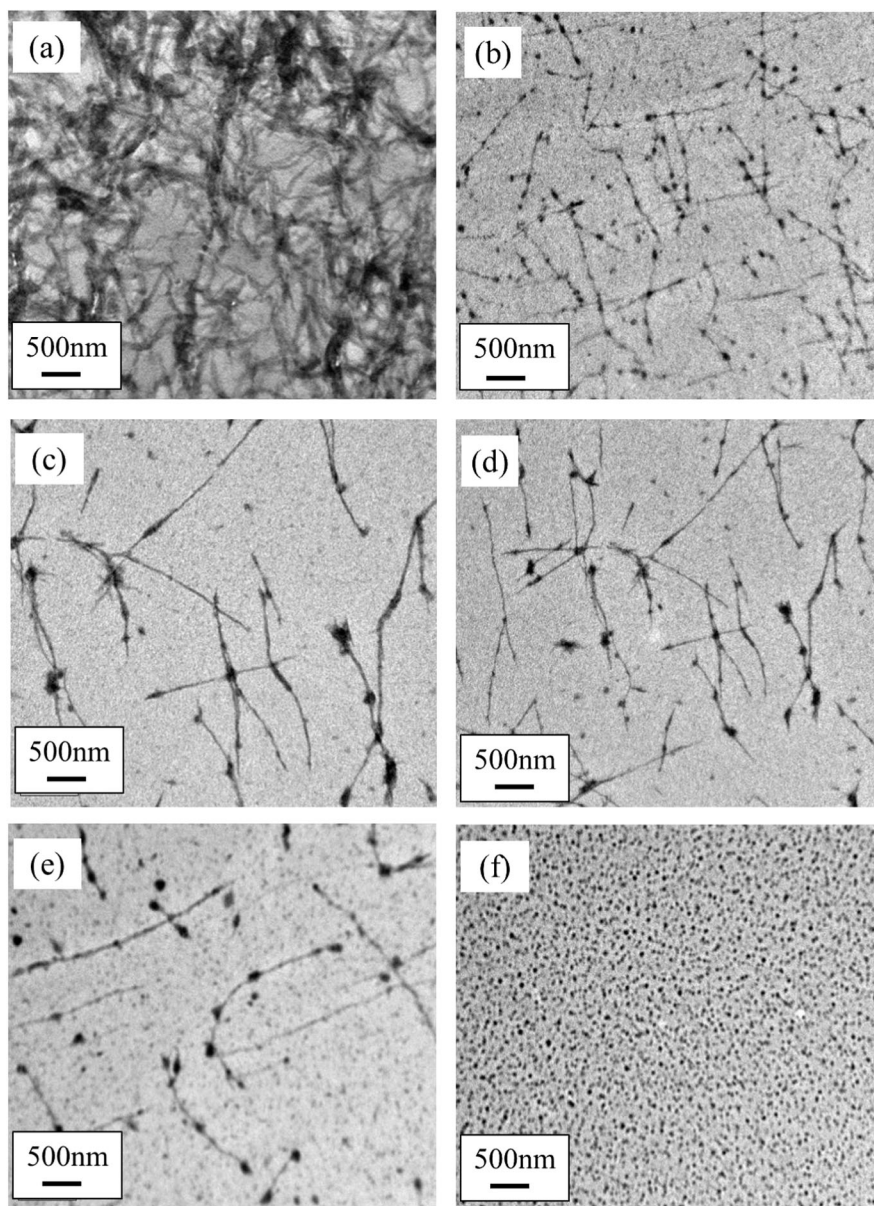
content of PLA was increased from 0 wt% to 99 wt%. However, these two shoulder peaks are also observed in the spectra of a few blends with ratios of 1% P3HT. These results indicate that a large proportion of the P3HT molecules in CH$_2$Cl$_2$ may have solidified to form nanowires. Therefore, according to the optical absorption results of the solution-type blends and thin-film-type blends, P3HT exhibited superior molecular packing of polymer chains in CH$_2$Cl$_2$ over that in CHCl$_3$.

Morphology analysis (SEM)

Device performance was highly dependent on the P3HT content in the blend film. Hence, the characteristics of the OFETs were highly related to the morphology of the P3HT/

PLA-blend thin film. To investigate the morphology of this phase, we spin-coated CH$_2$Cl$_2$ and CHCl$_3$ solutions onto the PTS-treated SiO$_2$/Si substrate. The spin-coated PTS was then modified on a SiO$_2$ surface to simulate the OFET structure. Before measurement, Pt was sputtered onto the samples. The surface morphologies of the P3HT/PLA-blend thin films were examined using SEM (Figs. 2–4). As shown in Fig. 2, the morphology of the thin films with different blend ratios obtained from CHCl$_3$ differed considerably. Figure 2a shows an image of pristine P3HT, Fig. 2b shows that of the P3HT/PLA blend with a ratio of 90 wt%, and Fig. 2c shows that of the P3HT/PLA blend with a ratio of 70 wt%. P3HT showed a continuous phase-separation morphology. However, as the P3HT content decreased to 50 wt%, a change in the morphology of P3HT to isolated

Table 1 Electrical properties of P3HT/PLA-blend-based OFET devices made from $CHCl_3$ and CH_2Cl_2 solvent

P3HT (wt%)	CHCl$_3$			CH$_2$Cl$_2$		
	Mobility[a] (cm^2 Vs^{-1})	On/off (−)	V_{TH} (V)	Mobility[a] (cm^2 Vs^{-1})	On/off (−)	V_{TH} (V)
100	$(1.69 \pm 0.18) \times 10^{-3}$	2.20×10^1	23 ± 1	$(5.80 \pm 0.39) \times 10^{-3}$	4.33×10^1	98 ± 2
90	$(2.24 \pm 0.29) \times 10^{-3}$	2.14×10^3	6 ± 3	$(5.26 \pm 0.52) \times 10^{-3}$	1.31×10^2	88 ± 6
70	$(7.77 \pm 0.19) \times 10^{-4}$	3.30×10^2	-6 ± 3	$(6.58 \pm 0.24) \times 10^{-3}$	3.90×10^2	67 ± 6
50	3.68×10^{-7}	5.9	27	$(5.75 \pm 0.87) \times 10^{-3}$	6.15×10^2	43 ± 2
30	–	–	–	$(6.41 \pm 0.70) \times 10^{-3}$	6.75×10^2	27 ± 2
10	–	–	–	$(5.30 \pm 0.93) \times 10^{-3}$	3.23×10^3	4 ± 5
5	–	–	–	$(1.88 \pm 0.82) \times 10^{-3}$	4.00×10^3	4 ± 3
2	–	–	–	$(1.76 \pm 0.43) \times 10^{-3}$	3.20×10^4	-22 ± 5
1	–	–	–	$(1.78 \pm 0.96) \times 10^{-4}$	1.44×10^4	-12 ± 3

[a]Average values obtained for at least three devices

spherical domains with a diameter of approximately 500 nm in the PLA matrix was observed (Fig. 2d). Figures 3 and 4 show the dramatic change that occurs in the morphology of the thin film obtained from CH_2Cl_2: for P3HT blend ratios from 100 wt% (Fig. 3a) to 50 wt% (Fig. 3d) and from 30 wt% (Fig. 4) to 2 wt%, a network of P3HT nanowires with an average diameter of approximately 30 nm was observed. Intriguingly, thin-film-type P3HT/PLA blends with 2 wt% P3HT exhibited straight nanowires. Although the nanofibers were less dense at lower P3HT contents, an interconnected network could still be achieved, even at P3HT contents as low as 1 wt%. Such networks may ensure the connectivity of conducting channels between the source and drain electrodes. The differences in the surface morphologies of the P3HT/PLA blends between $CHCl_3$ and CH_2Cl_2 may be due to the differences in the solubility of P3HT in the two solvents. Previous papers reported that the solubility parameters of P3HT, PLA, $CHCl_3$, and CH_2Cl_2 are 19.3, 20.8, 19.0, and 20.3 MPa$^{0.5}$, respectively [45–47]. Thus, $CHCl_3$ is a better solvent than CH_2Cl_2 for P3HT. P3HT dissolution in CH_2Cl_2 was relatively difficult. To fully dissolve P3HT in CH_2Cl_2 and subsequently induce the crystallization of P3HT, the solutions were heated at 60 °C for 1 h and then cooled to room temperature over 12 h. Large-scale crystalline P3HT formed in the solutions, and thus, P3HT formed a nanowire morphology in the solution state. From the SEM images shown in Figs. 2–4, we could identify only the surface morphology of the thin films with various blend ratios. TEM images were required to examine the detailed P3HT phase-separated domains within the PLA matrix.

Morphology analysis (TEM)

The interior structures of the P3HT/PLA-blend thin films were observed using TEM (Figs. 5–7). The thin films were spin-coated from $CHCl_3$ and CH_2Cl_2 solutions onto a copper mesh. In the TEM images, the dark domain indicates P3HT, because P3HT has a higher electron density than PLA. As shown in Fig. 5a, b, the P3HT domain exhibited a continuous phase-separation morphology when the blend ratio was 100–90 wt%. A bicontinuous network of P3HT and PLA was observed in the blend film containing comparable amounts of the two components (70:30, Fig. 5c) [17, 29]. When the P3HT content was decreased to 50%, isolated spherical structures with diameters of approximately 500 nm in the PLA matrix were obtained (Fig. 5d). Figures 6 and 7 show the TEM phase images of P3HT/PLA blends prepared from CH_2Cl_2 containing P3HT at various ratios. For blend ratios from 100 wt% (Fig. 6a) to 2 wt% (Fig. 7d), networks of P3HT nanowires with average diameters of approximately 30 nm were formed. The number of nanowires was lower on the surfaces with lower P3HT content. Even at 2 wt% P3HT, a few fiber-like P3HT domains and their network structures can be identified in the TEM image shown in Fig. 7d. The blend containing 1 wt% P3HT contained short nanowires and isolated spherical aggregates, suggesting improved solubility for small amounts of P3HT in CH_2Cl_2 (Fig. 7e). The crystalline P3HT formed nanowires in the CH_2Cl_2 solution after the heating and cooling process because CH_2Cl_2 is a poor solvent for P3HT. These properties suggest that P3HT/PLA blends could form a network of nanowires even at low P3HT content. The results of the TEM images were the same as those of the SEM images. The one-dimensional nanowire morphology may provide an efficient pathway for charge transport in OFETs.

Characterization of OFETs

CH_2Cl_2, a marginal solvent for P3HT, and $CHCl_3$, a good solvent for P3HT, were used as solvents to observe the differences in OFET performance. Solutions of P3HT/PLA blends of various ratios, each with a total concentration of 10 mg mL^{-1}, were prepared using $CHCl_3$ and CH_2Cl_2. Thin films were then deposited on PTS-treated silicon substrates by spin-coating. The field-effect mobility in the saturation

regime at $V_{DS} = -100$ V was recorded to investigate charge transport and reduce the influence of traps. The transfer and output characteristics of the OFETs were determined using a Keithley 4200 semiconductor parametric analyzer.

The dependence of the carrier transport mobility on the P3HT/PLA blend ratio for the $CHCl_3$ and CH_2Cl_2 solutions is detailed in Table 1, and the transfer characteristics of the FETs based on P3HT/PLA blends spin-cast from $CHCl_3$ and CH_2Cl_2 are shown in Fig. 8a, b, respectively. Solvent influence was discovered to result in significant differences in charge carrier mobility. Figure 8c illustrates a clear decline in the charge carrier mobility of OFETs fabricated from $CHCl_3$ as the P3HT content decreased. Furthermore, the charge carrier mobility was difficult to measure when the P3HT/PLA-blend ratio was 1:1 due to a small current and unstable transfer characteristics. The TEM image of the 1:1 P3HT/PLA blend (Fig. 5d) shows that the P3HT domain contained isolated spherical structures with diameters of approximately 500 nm in the PLA matrix. Thus, the mobility was dramatically lower at 50 wt% P3HT than at 100–70 wt% P3HT. The field-effect characteristics and morphology results clearly reveal that a decrease in the connectivity of the P3HT phase causes degradation of the electronic properties in $CHCl_3$-based P3HT/PLA solutions with low P3HT content.

Conversely, the charge carrier mobility of OFETs fabricated from CH_2Cl_2 changed only slightly as the content of P3HT decreased from 100 wt% to 10 wt%. The film with 10 wt% P3HT had an average mobility of 5.30×10^{-3} cm^2 $(Vs)^{-1}$, which was similar to that of the pristine P3HT film $(5.80 \times 10^{-3}$ cm^2 $(Vs)^{-1})$ under the same processing conditions. Lower mobility was observed in the OFETs with P3HT contents less than 10 wt%. We observed similarly high mobility at P3HT contents from 100 wt% to 10 wt%, and the same order mobility was observed even at P3HT contents as low as 2 wt%. The 2 wt% P3HT film had an average mobility of 1.76×10^{-3} cm^2 $(Vs)^{-1}$, which is only three times smaller than that of the pristine P3HT film $(5.80 \times 10^{-3}$ cm^2 $(Vs)^{-1})$ under the same processing conditions. This stable electronic performance resulted from the network structure of P3HT nanowires with average diameters of approximately 30 nm that formed when the blend ratio ranged from 100 wt% to 2 wt% P3HT, as observed in the TEM images (Fig. 6 and Fig. 7). Even at 2 wt% P3HT, a few fiber-like P3HT domains and their network structures were found (Fig. 7d). However, decreased mobility was observed for the OFETs with P3HT contents lower than 2 wt%, and when the P3HT content was 1 wt%, the mobility was only 1.78×10^{-4} cm^2 $(Vs)^{-1}$. These findings indicate that the percolation threshold of the P3HT/PLA blends is less than 1 wt% P3HT, which is among the lowest values reported for OFETs based on polymer blends [32, 48]. The TEM images in Fig. 7 show the one-dimensional P3HT
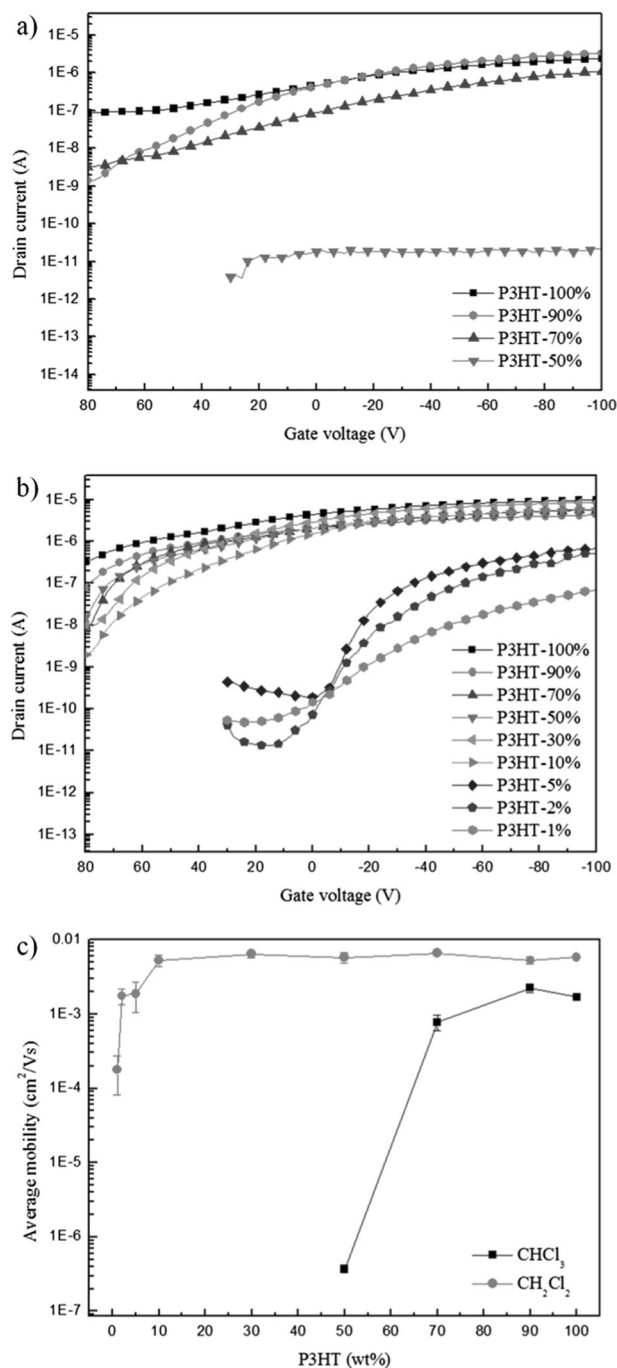
Fig. 8 Transfer characteristics of an OFET based on a P3HT/PLA blend prepared from **a** $CHCl_3$ and **b** CH_2Cl_2. **c** Variation in OFET mobility as a function of P3HT content in P3HT/PLA blends fabricated from $CHCl_3$ and CH_2Cl_2 solutions

nanowire morphology, which provided an efficient pathway for OFET charge transport. Because of this nanowire morphology, the OFETs still exhibited charge mobility when the P3HT content was as low as 1 wt%. The on/off ratio was discovered to increase as P3HT content decreased from 100 to 2 wt% but then decreased when the P3HT content was decreased to 1 wt%. The threshold (gate) voltage declined
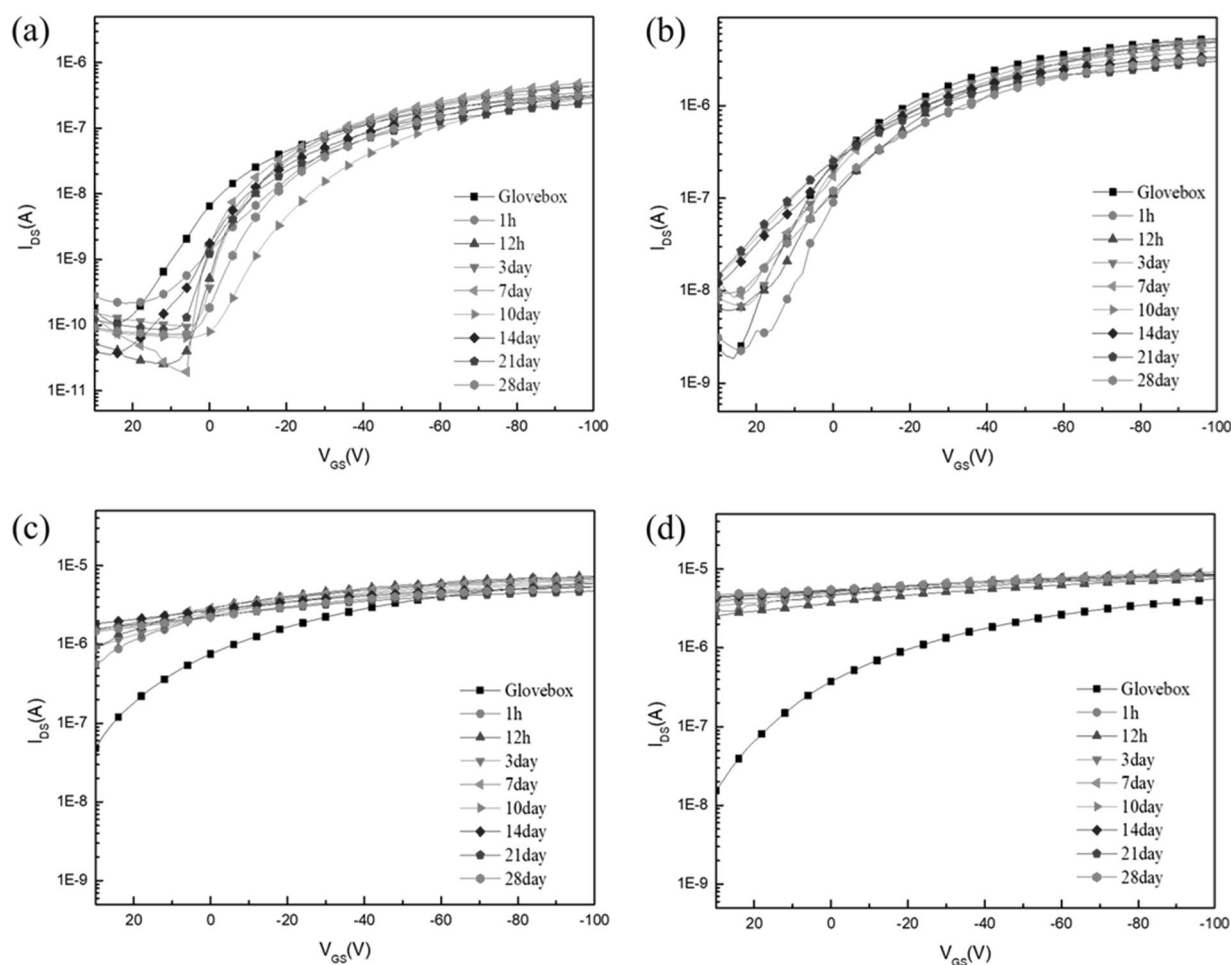
Fig. 9 Transfer characteristics as a function of time for devices exposed to air, where the P3HT content of the P3HT/PLA blend in CH_2Cl_2 was **a** 2%, **b** 10%, **c** 50%, and **d** 100%

as the PLA content increased. These results are consistent with earlier reported results [29, 32, 33], wherein PLA, acting as an insulator, lowered the current density and reduced the pathway for charge carriers. Additionally, the threshold voltages and the on/off ratios of the P3HT/PLA-blend OFETs improved significantly with increased PLA content, possibly because the insulating PLA provided a kinetic barrier against the invasion of oxygen and moisture. Thus, the P3HT/PLA device could maintain a high on-current without obvious degradation, even when the content of P3HT was as low as 2 wt%. These results indicate that OFET performance can be maintained using only a small amount of P3HT in P3HT/PLA blends.

Air stability

The poor air stability of p-type semiconductors, such as pristine P3HT, originates from the high-lying Highest occupied molecular orbital (HOMO) levels, which are easily doped in ambient atmosphere [29]. This restriction

can be overcome by using an insulating, biodegradable, and green polymer, PLA, to encapsulate P3HT nanowires and reduce the influence of the ambient atmosphere. Representative output and transfer characteristics over a period of air exposure for OFETs based on P3HT/PLA blends of various ratios are shown in Fig. 9. Air stability testing of P3HT/PLA blends was performed by measuring the mobility, on/off current ratio, and threshold voltage (V_{th}), as shown in Fig. 10. The transfer characteristics of samples with four blend ratios (2, 10, 50, and 100 wt% P3HT) over 28 days of air exposure were monitored as functions of time using a Keithley 4200 semiconductor parametric analyzer; the results are presented in Figs. 9a (2%), 9b (10%), 9c (50%), and 9d (100%). Device performance in air varied depending on the relative humidity [23]. In this study, the relative humidity ranged from 45 to 65%. As shown in Fig. 10a, the mobility of the 10/90 P3HT/PLA blend decreased slightly from 5.3×10^{-3} cm^2 (Vs)$^{-1}$ (in a glove box) to 3.7×10^{-3} cm^2 (Vs)$^{-1}$ (after air exposure for 28 days), and the mobility in pristine P3HT decreased by
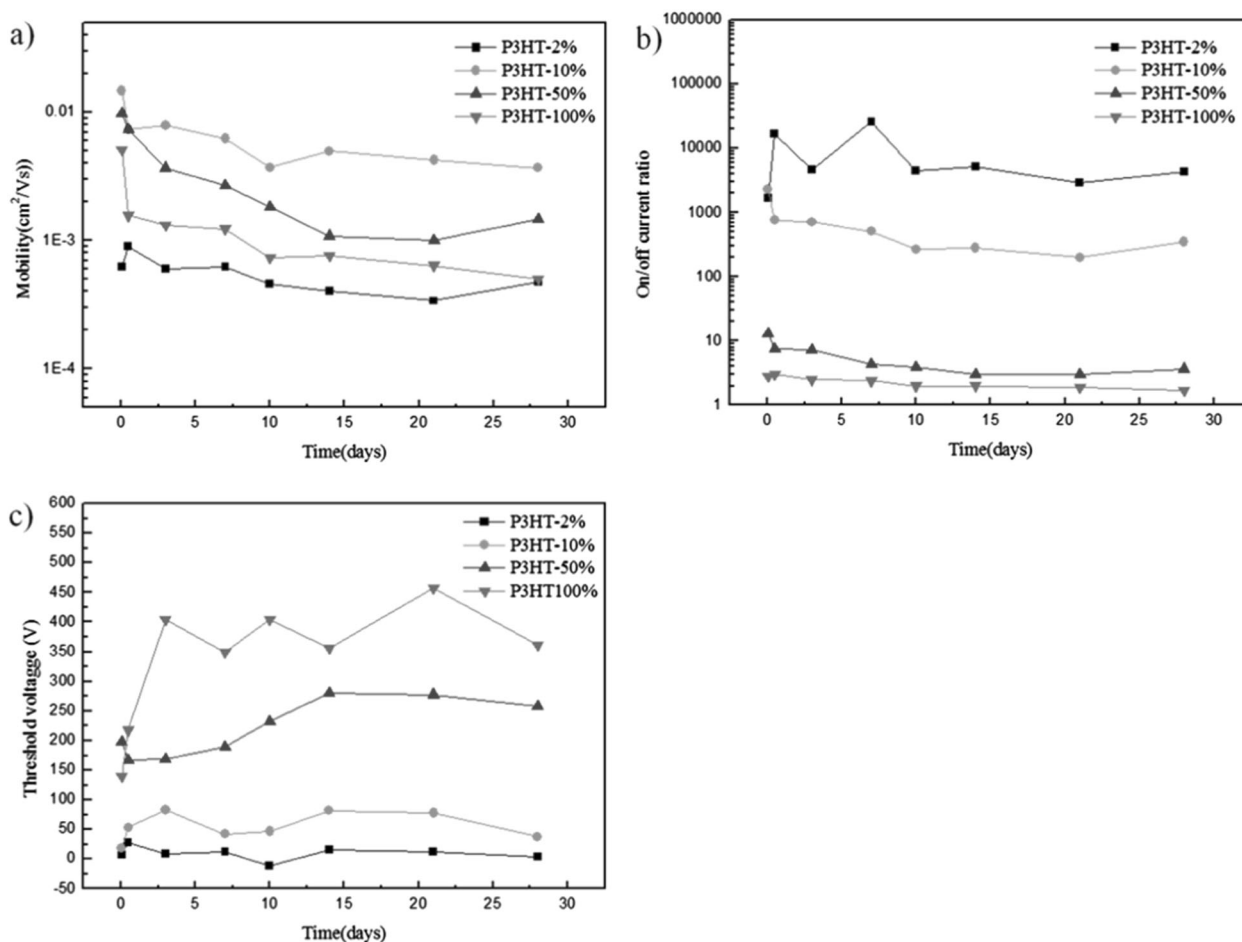
Fig. 10 Air stability testing of the characteristics of an FET containing a P3HT/PLA blend prepared from CH_2Cl_2 solution: **a** mobility, **b** on/off ratio, and **c** threshold voltage. The samples are for four P3HT/PLA-blend ratios (2, 10, 50, and 100 wt% P3HT)

approximately one order of magnitude. The on/off ratio of the devices remained stable as the PLA content increased. The 2 wt% P3HT/PLA-blend device had a favorable on/off ratio of 4.4×10^3 after 28 days of exposure in air, and the on/off ratio of pristine P3HT decreased dramatically by one order of magnitude. Thus, insulating PLA was shown to protect encapsulated P3HT nanowires from oxygen and water (Fig. 10b). After 28 days of air exposure, the threshold voltage in devices with 2, 10, 50, and 100 wt% P3HT content was 4, 38, 258, and 361 V, respectively (Fig. 10c). The large positive shift in the V_{th} value that was measured when the content of P3HT was 100% may be due to the numerous grain boundaries on the surfaces serving as channels for the diffusion of oxygen and moisture, which would otherwise act as electron traps in active channel layers. The large positively shifted V_{th} indicated a significant reduction in the OFET device performance when a pristine P3HT film was used in an ambient atmosphere. Hence, the P3HT/PLA blend improved the air stability of the device. Our results confirm that we successfully

prepared green-polymer-blended OFETs that exhibited high charge mobility and air stability and were based on low-P3HT-content blends with the biodegradable and green polymer PLA.

Conclusions

In this study, we demonstrated the morphology and effects on the OFET performance of blends of various ratios of P3HT and insulating PLA using $CHCl_3$ and CH_2Cl_2 as solvents. When the marginal solvent CH_2Cl_2 was used, high carrier mobility was maintained at P3HT levels ranging from 100 to 10 wt%, and the on/off current ratio increased with increasing PLA content. The P3HT/PLA-blend, nanowire-based OFETs exhibited high hole mobility. Even at 2 wt% P3HT, the mobility was $1.76 \times 10^{-3} \, cm^2 \, (Vs)^{-1}$. However, the mobility in the P3HT/PLA blends in $CHCl_3$ decreased dramatically when the P3HT content was reduced from 100 to 50 wt%. In CH_2Cl_2, P3HT formed fiber-like

network structures, whereas SEM and TEM analysis revealed isolated spherical domains when $CHCl_3$ solvent was employed. Therefore, we concluded that a P3HT network structure within the PLA matrix could be induced using CH_2Cl_2. The one-dimensional nanowire morphology of these network structures may have provided an efficient pathway for OFET charge transport. In addition, the P3HT nanowires were embedded in the PLA matrix, thereby reducing P3HT contact with the atmosphere and resulting in high environmental stability. Thus, OFETs based on P3HT/ PLA blends exhibited greater environmental stability than those based only on P3HT, because in the blend systems, a PLA matrix served as an efficient kinetic barrier to ambient atmosphere influence. These results confirm that P3HT/ PLA blends in CH_2Cl_2 solvent could be used to fabricate low-cost, green-polymer-blended FETs.

Compliance with ethical standards

Conflict of interest The authors declare that they have no conflict of interest.

References

1. Lin HW, Lee WY, Lu C, Lin CJ, Wu HC, Lin YW, Ahn B, Rho Y, Ree M, Chen WC. Biaxially extended quaterthiophene-thiophene and -selenophene conjugated polymers for optoelectronic device applications. Polym Chem. 2012;3:767–77.
2. Lee WY, Cheng KF, Wang TF, Chueh CC, Chen WC, Tuan CS, Lin JL. Effects of acceptors on the electronic and optoelectronic properties of fluorene-based donor–acceptor–donor copolymers. Macromol Chem Phys. 2007;208:1919–27.
3. Zaumseil J, Sirringhaus H. Electron and ambipolar transport in organic field-effect transistors. Chem Rev. 2007;107:1296–323.
4. Murphy AR, Fréchet JMJ. Organic semiconducting oligomers for use in thin film transistors. Chem Rev. 2007;107:1066–96.
5. Dimitrakopoulos CD, Malenfant PRL. Organic thin film transistors for large area electronics. Adv Mater. 2002;14:99–117.
6. Katz HE. Recent advances in semiconductor performance and printing processes for organic transistor-based electronics. Chem Mater. 2004;16:4748–56.
7. Lin HW, Lee WY, Chen WC. Selenophene-DPP donor–acceptor conjugated polymer for high performance ambipolar field effect transistor and nonvolatile memory applications. J Mater Chem. 2012;22:2120–8.
8. Wang C, Dong H, Hu W, Liu Y, Zhu D. Semiconducting pi-conjugated systems in field-effect transistors: a material odyssey of organic electronics. Chem Rev. 2012;112:2208–67.
9. Sirringhaus H, Brown PJ, Friend RH, Nielsen MM, Bechgaard K, Langeveld-Voss BMW, Spiering AJH, Janssen RAJ, Meijer EW, Herwig P, de Leeuw DM. Two-dimensional charge transport in self-organized, high-mobility conjugated polymers. Nature. 1999;401:685–8.
10. Huitema HEA, Gelinck GH, van der Putten JBPH, Kuijk KE, Hart KM, Cantatore E, de Leeuw DM. Active-matrix displays driven by solution processed polymeric transistors. Adv Mater. 2002;14:1201–4.
11. Janata J, Josowicz M. Conducting polymers in electronics chemical sensors. Nat Mater. 2003;2:19–24.
12. Dodabalapur A. Organic and polymer transistors for electronics. Mater Today. 2006;9:24–30.
13. Huitema HEA, Gelinck GH, J. van der Putten BPH, Kuijk KE, Hart CM, Cantatore E, Herwig PT, van Breemen AJJM, de Leeuw DM. Plastic transistors in active-matrix displays. Nature. 2001;414:598–9.
14. Böhm M, Ullmann A, Zipperer D, Knobloch A, Glauert WH, Fix W. Printable electronics for polymer RFID applications. IEEE Int Conf Electron Devices Solid-State Circuits. 2006;1034–41.
15. Kline RJ, McGehee MD, Kadnikova EN, Liu JS, Frechet JMJ. Controlling the field-effect mobility of regioregular polythiophene by changing the molecular weight. Adv Mater. 2003;15:1519–22.
16. Kline RJ, McGehee MD, Kadnikova EN, Liu JS, Frechet JMJ, Toney MF. Dependence of regioregular poly(3-hexylthiophene) film morphology and field-effect mobility on molecular weight. Macromolecules. 2005;38:3312–19.
17. Chen JY, Kuo CC, Lai CS, Chen WC, Chen HL. Manipulation on the morphology and electrical properties of aligned electrospun nanofibers of poly(3-hexylthiophene) for field-effect transistor applications. Macromolecules. 2011;44:2883–92.
18. Lee YH, Yen WC, Su WF, Dai CA. Self-assembly and phase transformations of π-conjugated block copolymers that bend and twist: from rigid-rod nanowires to highly curvaceous gyroids. Soft Matter. 2011;7:10429–42.
19. Dong H, Fu X, Liu J, Wang Z, Hu W. 25th anniversary article: key points for high-mobility organic field-effect transistors. Adv Mater. 2013;25:6158–83.
20. Miozzo L, Yassar A, Horowitz G. Surface engineering for high performance organic electronic devices: the chemical approach. J Mater Chem. 2010;20:2513–38.
21. Zhao K, Ding Z, Xue L, Han Y. Crystallization-induced phase segregation based on double-crystalline blends of poly(3-hexylthiophene) and poly(ethylene glycol)s. Macromol Rapid Commun. 2010;31:532–8.
22. Babel A, Jenekhe SA. Charge carrier mobility in blends of poly (9,9-dioctylfluorene) and poly(3-hexylthiophene). Macromolecules. 2003;36:7759–64.
23. Kumar A, Baklar MA, Scott K, Kreouzis T, Stingelin-Stutzmann N. Efficient, stable bulk charge transport in crystalline/crystalline semiconductorâ insulator blends. Adv Mater. 2009;21:4447–51.
24. Russell DM, Newsome CJ, Li SP, Kugler T, Ishida M, Shimoda T. Blends of semiconductor polymer and small molecular crystals for improved-performance thin-film transistors. Appl Phys Lett. 2005;87:222109.
25. Sparrowe D, Baklar M, Stingelin N. Low-temperature printing of crystalline:crystalline polymer blend transistors. Org Electron. 2010;11:1296–1300.
26. Babel A, Jenekhe SA. Field-effect mobility of charge carriers in blends of regioregular poly(3-alkylthiophene)s. J Phys Chem B. 2003;107:1749–54.
27. Lee WY, Giri G, Diao Y, Tassone CJ, Matthews JR, Sorensen ML, Mannsfeld SCB, Chen WC, Fong HH, Tok JBH, Toney MF, He M, Bao Z. Effect of non-chlorinated mixed solvents on charge transport and morphology of solution-processed polymer field-effect transistors. Adv Funct Mater. 2014;24:3524–34.
28. Nicho ME, García-Escobar CH, Arenas MC, Altuzar-Coello P, Cruz-Silva R, Güizado-Rodríguez M. Influence of P3HT concentration on morphological, optical and electrical properties of P3HT/PS and P3HT/PMMA binary blends. Mater Sci Eng B. 2011;176:1393–1400.

29. Qiu L, Lee WH, Wang X, Kim JS, Lim JA, Kwak D, Lee S, Cho K. Organic thin-film transistors based on polythiophene nanowires embedded in insulating polymer. Adv Mater. 2009;21:1349–53.

30. Lee Y, Kim JK, Chiu CH, Lan YK, Huang CI. Phase behavior of poly (3-alkylthiophene)/polystyrene blends. Polymer. 2009;50:4944–49.

31. Kergoat L, Battaglini N, Miozzo L, Piro B, Pham MC, Yassar A, Horowitz G. Use of poly(3-hexylthiophene)/poly(methyl methacrylate) (P3HT/PMMA) blends to improve the performance of water-gated organic field-effect transistors. Org Electron. 2011; 12:1253–57.

32. Goffri S, Muller C, Stingelin-Stutzmann N, Breiby DW, Radano CP, Andreasen JW, Thompson R, Janssen RAJ, Nielsen MM, Smith P, Sirringhaus H. Multicomponent semiconducting polymer systems with low crystallization-induced percolation threshold. Nat Mater. 2006;5:950–6.

33. Babel A, Jenekhe SA. Morphology and field-effect mobility of charge carriers in binary blends of poly(3-hexylthiophene) with poly[2-methoxy-5-(2-ethylhexoxy)-1,4-phenylenevinylene] and polystyrene. Macromolecules. 2004;37:9835–40.

34. Lee SW, Lee HJ, Choi JH, Koh WG, Myoung JM, Hur JH, Park JJ, Cho JH, Jeong U. Periodic array of polyelectrolyte-gated organic transistors from electrospun poly(3-hexylthiophene) nanofibers. Nano Lett. 2010;10:347–51.

35. Qiu L, Lim JA, Wang X, Lee WH, Hwang M, Cho K. Versatile use of vertical-phase-separation-induced bilayer structures in organic thin-film transistors. Adv Mater. 2008;20:1141–5.

36. Lin JC, Lee WY, Wu HC, Chou CC, Chiu YC, Sun YS, Chen WC. Morphology and field-effect transistor characteristics of semicrystalline poly(3-hexylthiophene) and poly(stearyl acrylate) blend nanowires. J Mater Chem. 2012;22:14682.

37. Lee S, Jeon H, Jang M, Baek KY, Yang H. Tunable solubility parameter of poly(3-hexyl thiophene) with hydrophobic sidechains to achieve rubbery conjugated films. ACS Appl Mater Interfaces. 2015;7:1290–7.

38. Shikinami Y, Okuno M. Bioresorbable devices made of forged composites of hydroxyapatite (HA) particles and poly l-lactide (PLLA). Part II: practical properties of miniscrews and miniplates. Biomaterials. 2001;22:3197–211.

39. Tsuji H. In vitro hydrolysis of blends from enantiomeric poly (lactide)s. Part 4: well-homo-crystallized blend and nonblended films. Biomaterials. 2003;24:537–47.

40. Li S, Vert M. Synthesis, characterization, and stereocomplex-induced gelation of block copolymers prepared by ring-opening polymerization of L(D)-lactide in the presence of poly(ethylene glycol). Macromolecules. 2003;36:8008–14.

41. Ho V, Boudouris BW, McCulloch BL, Shuttle CG, Burkhardt M, Chabinyc ML, Segalman RA. Poly(3-alkylthiophene) diblock copolymers with ordered microstructures and continuous semi-conducting pathways. J Am Chem Soc. 2011;133:9270–3.

42. Grancharov G, Coulembier O, Surin M, Lazzaroni R, Dubois P. Stereocomplexed materials based on poly(3-hexylthiophene)-b-poly(lactide) block copolymers: synthesis by organic catalysis, thermal properties, and microscopic morphology. Macromolecules. 2010;43:8957–64.

43. Smith J, Hamilton R, McCulloch I, Stingelin-Stutzmann N, Heeney M, Bradley DDC, Anthopoulos TD. Solution-processed organic transistors based on semiconducting blends. J Mater Chem. 2010;20:2562–74.

44. Brown PJ, Thomas DS, Köhler A, Wilson JS, Kim JS, Ramsdale CM, Sirringhaus H, Friend RH. Effect of interchain interactions on the absorption and emission of poly(3-hexylthiophene). Phys Rev B. 2003;67:064203. 1-16

45. Machui F, Abbott S, Waller D, Koppe M, Brabec CJ. Determination of solubility parameters for organic semiconductor formulations. Macromol Chem Phys. 2011;212:2159–65.

46. Thomasin C, Merkle HP, Gander B. Drug microencapsulation by PLA/PLGA coacervation in the light of thermodynamics. 2. Parameters determining microsphere formation. J Pharm Sci. 1998;87:269–75.

47. Ham HT, Choi YS, Chung IJ. An explanation of dispersion states of single-walled carbon nanotubes in solvents and aqueous surfactant solutions using solubility parameters. J Colloid Interface Sci. 2005;286:216–23.

48. Chiu MY, Jeng US, Su MS, Wei KH. Morphologies of self-organizing regioregular conjugated polymer/fullerene aggregates in thin film solar cells. Macromolecules. 2010;43:428–32.